ResearchGate

See discussions, stats, and author profiles for this publication at: https://www.researchgate.net/publication/244447149

Flow Induced Crystallization in Isotactic Polypropylene1,3:2,4Bis(3,4-dimethylbenzylidene)sorbitol Blends: Implications on Morphology of Shear and Phase Separation

ARTICLE *in* MACROMOLECULES · JANUARY 2008

Impact Factor: 5.8 · DOI: 10.1021/ma071460g

CITATIONS
57

READS
47

3 AUTHORS, INCLUDING:

Sanjay Rastogi
Maastricht University
165 PUBLICATIONS **2,947** CITATIONS
SEE PROFILE

Gerrit W M Peters
Technische Universiteit Eindhoven
337 PUBLICATIONS **5,411** CITATIONS
SEE PROFILE

Available from: Gerrit W M Peters
Retrieved on: 25 January 2016

Flow Induced Crystallization in Isotactic Polypropylene−1,3:2,4-Bis(3,4-dimethylbenzylidene)sorbitol Blends: Implications on Morphology of Shear and Phase Separation

Luigi Balzano,[†,‡] Sanjay Rastogi,*[,†,‡,§] and Gerrit W. M. Peters[‡,||]

Department of Chemical Engineering and Department of Mechanical Engineering, Eindhoven University of Technology, P.O. Box 513, 5600 MB Eindhoven, The Netherlands, Institute of Polymer Technology and Materials Engineering (IPTME), Loughborough University, Loughborough, LE11 3TU, United Kingdom, and Dutch Polymer Institute (DPI), P.O. Box 902, 5600 AX Eindhoven, The Netherlands

Received July 2, 2007; Revised Manuscript Received November 4, 2007

ABSTRACT: Nucleation is the limiting stage in the kinetics of polymer crystallization. In many applications of polymer processing, nucleation is enhanced with the addition of nucleating agents. 1,3:2,4-Bis(3,4-dimethylbenzylidene)sorbitol or DMDBS is a nucleating agent tailored for isotactic polypropylene (iPP). The presence of DMDBS changes the phase behavior of the polymer. For high enough temperatures, the system iPP−DMDBS forms a homogeneous solution. However, in the range of concentration spanning from 0 to 1 wt % of DMDBS, the additive can phase separate/crystallize above the crystallization temperature of the polymer, forming a percolated network of fibrils. The surface of these fibrils hosts a large number of sites tailored for the nucleation of iPP. The aim of this paper is to investigate the combined effect of flow and DMDBS phase separation on the morphology of iPP. To this end, we studied the rheology of phase separated iPP−DMDBS systems and its morphology with time-resolved small-angle X-ray scattering (SAXS). The effect of flow is studied combining rheology, SAXS, and a short-term shear protocol. We found that, with phase separation, DMDBS forms fibrils whose radius (∼5 nm) does not depend on the DMDBS concentration. The growth of these fibrils leads to a percolated network with a mesh size depending on DMDBS concentration. Compared to the polymer, the relaxation time of the network is quite long. A shear flow, of 60 s^{-1} for 3 s, is sufficient to deform the network and to produce a long-lasting alignment of the fibrils. By design, lateral growth of iPP lamellae occurs orthogonally to the fibril axis. Therefore, with crystallization, the preorientation of DMDBS fibrils is transformed into the orientation of the lamellae. This peculiarity is used here to design thermomechanical histories for obtaining highly oriented iPP morphologies after shearing well above the melting point of the polymer (i.e., without any undercooling). In contrast, when shear flow is applied prior to DMDBS crystallization, SAXS showed that iPP crystallization occurs with isotropic morphologies.

1. Introduction

Morphology control is an important issue in polymer processing as it influences a broad range of properties of the final products. For instance, mechanical, optical, and transport properties of polymeric materials depend on the size and shape of the crystallites.[1,2] It is well-known that thermal and mechanical histories do play an important role in the creation of these morphological features[3,4] and that additives can also have a remarkable influence.[2,5−8] Nucleating agents are a family of additives used to speed up processing rates of polymers. In the case of isotactic polypropylene (iPP), a common nucleating agent is a sorbitol derivative: 1,3:2,4-bis(3,4-dimethylbenzylidene)sorbitol or DMDBS. DMDBS is a chiral molecule that, driven by hydrogen bonding, can self-assemble into fibrillar structures. Crystallization of DMDBS within the iPP matrix corresponds to a liquid−solid phase separation, in the following, referred to as DMDBS crystallization or DMDBS phase separation. The DMDBS molecule has a special "butterfly" configuration, see Figure 1. The "wings" of the molecule (phenyl rings with two methyl groups attached) enable dissolution in the polymer and, at the same time, are tailored nucleation sites for iPP, while the "body" comprises two moieties: one dictates the geometry of the molecule and the other bears the polar groups (hydroxyls) for hydrogen bond formation.[9] Polarity is, therefore, one of the main features of DMDBS. In contrast, iPP is a fully apolar molecule. This difference becomes clear and leads to a rich phase diagram when iPP and DMDBS are compounded together.

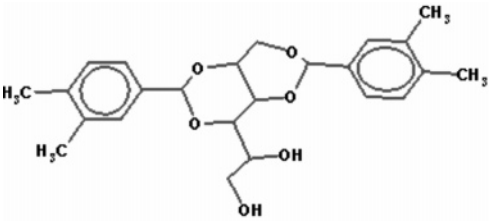

Figure 1. Chemical structure of DMDBS.

Kristiansen et al.[10] proposed a monotectic model for this phase diagram where the eutectic point lies around 0.15 wt % of the additive. In their model, miscibility of the two molecules is always possible at high temperatures. They define four concentration regimes based on different phase transitions occurring during the cooling of a homogeneous mixture. From the application point of view, the most interesting concentration regime is where the additive plays the role of clarifier enhancing

* To whom correspondence should be addressed.
† Department of Chemical Engineering, Eindhoven University of Technology.
‡ Dutch Polymer Institute.
§ Loughborough University.
|| Department of Mechanical Engineering, Eindhoven University of Technology.

10.1021/ma071460g CCC: $40.75 © 2008 American Chemical Society
Published on Web 12/19/2007

the transparency of the material. This happens above the eutectic point where a liquid−solid phase separation occurs as a consequence of the crystallization of DMDBS prior to the crystallization of the polymer. Under these conditions, DMDBS forms fibrils with a typical length of several microns and a radius that can reach 50 nm.[12] These fibrils connect and thus form a percolated network suspended in the polymer matrix. The nucleation sites for the polymer lie on the surface of this network. The fibrillar arrangement provides a high surface to volume (S/V) ratio and, therefore, provides a large number of nucleation sites per unit of volume. However, S/V alone cannot explain the nucleation ability of DMDBS. Thierry et al.[9] and Fillon et al.[11] demonstrated that DMDBS is a good nucleating agent for iPP because of a good lattice matching between its crystals and the 3_1 helix of the polymer. The same authors also define an efficiency scale for nucleating agents, ranging from 0 to 100%, based on characteristic crystallization temperatures. Dibenzylidene sorbitol (DBS), a nucleating agent very similar to DMDBS, was rated at 41%. Among several nucleating agents, they found that 4-biphenyl carboxylic acid (2 wt % in iPP) has the highest nucleation efficiency (66%).

The effect of several sorbitol based nucleating agents on quiescent crystallization kinetics and the morphology of iPP has been widely explored,[12−14] as was the rheology of these systems.[12,15,16] Surprisingly, little attention has been paid to the role of sorbitol based nucleating agents on the crystallization of iPP during or after imposition of a flow, the most common scenario in applications. A notable exception is the work of Nogales et al.[17,18] They studied the flow induced crystallization of iPP−DBS compounds after the phase separation of the additive under well-defined conditions, by means of both scattering and imaging techniques. For a concentration of 1 wt % DBS, they observed, during cooling, after application of modest shear flows (shear rates ranging from 0.1 to 20 s^{-1} at 170 °C), the formation of polymer morphologies characterized by high degrees of orientation.

However, the role of DMDBS phase separation in flow induced crystallization of iPP−DMDBS blends is not yet fully clarified and this is the main aim of this paper. The work includes also the changes in the rheology of the melt, associated with the formation of the DMDBS fibrillar network, and the flow behavior of this network. The results are based on a combination of Small-angle X-ray Scattering (SAXS), dynamic scanning calorimetry (DSC), and rheology. Four different iPP−DMDBS blends, containing 0, 0.3, 0.7, and 1.0 wt % of the additive are investigated in quiescent and flow conditions. We address three aspects of these blends: (1) crystallization without application of flow (quiescent conditions); (2) influence of flow prior to the crystallization of DMDBS; (3) influence of flow after crystallization of DMDBS.

2. Experimental Method

Materials. The iPP used in this work is a commercial homopolymer grade from Borealis GmbH (Austria), labeled HD120MO, with molecular weight, M_w, of 365.000 g/mol and a polydispersity, M_w/M_n, of 5.4. DMDBS (Millad 3988) was obtained in powder form from Milliken Chemicals (Gent, Belgium) and used as received.

Sample Preparation. The polymer, available in pellets, was first cryo-ground and then compounded with DMDBS in a corotating twin screw extruder (DSM, Geleen) for 10 min at temperatures ranging from 230 to 250 °C; the higher the DMDBS concentration the higher the compounding temperature used. To prevent degradation of both, polymer and additive, this operation was performed in a nitrogen rich atmosphere. The material obtained was compression molded with a hot press into films of different thicknesses: 1 mm for rheology and 200 μm for X-ray experiments. The compression molding temperature was 220 °C, and the molding time was 3 min. The resulting films were quenched to room temperature and cut in disklike samples. Following the same procedure, three blends of iPP with 0.3, 0.7, and 1 wt % of DMDBS were prepared. For convenience, these three blends are respectively renamed as B03, B07, and B1 in the text.

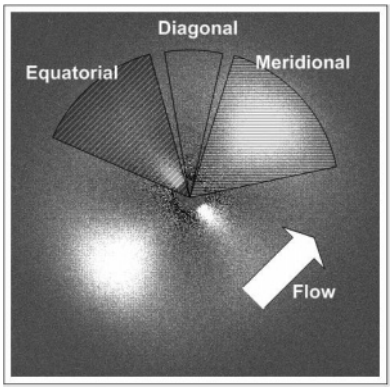

Figure 2. Anisotropic two-dimensional SAXS image with definitions of the azimuthal intensity regions. Arrow indicates the applied flow direction.

X-ray Characterization. X-ray characterization was done at the European Synchrotron Radiation Facility (ESRF) in Grenoble (France). Time-resolved small-angle X-ray scattering (SAXS) experiments were performed at beamline BM26/DUBBLE. Scattering patterns were recorded on a two-dimensional gas filled detector (512 × 512 pixels) placed at approximately 7.1 m from the sample. Scattering and absorption from air were minimized by a vacuum chamber placed between sample and detector. The wavelength adopted was $\lambda = 1.03$ Å. SAXS images were acquired with an exposure of 5 s and were corrected for the intensity of the primary beam, absorption, and sample thickness. The scattered intensity was integrated and plotted against the scattering vector, $q = (4\pi/\lambda)\sin(\vartheta/2)$ where ϑ is half of the scattering angle. The long period was calculated as $L_p = 2\pi/(q_{I_{MAX}})$, where $q_{I_{MAX}}$ is the q value corresponding to the maximum in the scattered intensity. Finally, we defined an integrated intensity as: $I_I = \int_{q_{min}}^{q_{max}} I(q)\mathrm{d}q$ where q_{min} and q_{max} are the minimum and the maximum experimentally accessible q values, respectively. Two-dimensional SAXS images were also used for the characterization of anisotropic morphologies. For this purpose, it was necessary to define three azimuthal regions.[19] The definitions adopted in the present work are given in Figure 2.

Shear flow experiments in combination with SAXS were carried out in a Linkam Shear Cell (CSS-450) modified with Kapton windows using a "short-term shearing" protocol. First, samples were annealed at 230 °C for 3 min to erase the memory of any previous thermomechanical treatment. Next, the temperature was decreased by 10 °C/min to the desired test temperature where flow was applied under isothermal conditions. For the purpose of this paper, we limit ourselves to the application of only one shear condition: nominal shear rate of 60 s^{-1} for 3 s. Finally, depending on the experimental requirements, the temperature was either decreased to the room temperature or kept constant.

Wide-angle X-ray scattering (WAXD) experiments were performed separately on beamline ID11 of the ESRF. The results were used to determine crystallinity and the phases present in the samples. Two-dimensional images were recorded on a Frelon detector. Before analysis, the scattering of air and of the empty sample holder was subtracted. After radial integration, the intensity was plotted as a function of the scattering angle 2ϑ. Deconvolution of the amorphous and crystalline scattered intensities was performed using a sixth order polynomial to capture the "amorphous halo".[20,21] The crystallinity index, a measure of the crystal volume fraction, was calculated as

$$X^{\mathrm{WAXD}} = \frac{A_{\mathrm{C}}}{A_{\mathrm{C}} + A_{\mathrm{A}}} \quad (1)$$

where A_A and A_C are the scattered intensities from the amorphous and the crystalline phases, respectively.

Rheological Characterization. Rheological measurements were performed in the linear viscoelastic regime using a strain-controlled ARES rheometer equipped with a 2KFRT force rebalance transducer. In all cases a plate−plate geometry with a diameter of 8 mm was used. Appropriate values of strain were determined with amplitude sweep tests carried out at 5 rad/s over a broad range of strains (ranging from 0.01 to 100%).[22]

During the study of phase transitions, large strains can enhance the process and/or affect the morphology.[23] These effects are minimized by using strains as low as 0.5% in the experiments.

DSC. The crystallization behavior of the three binary blends iPP−DMDBS was studied in quiescent conditions using dynamic scanning calorimetry. Samples of approximately 2 mg were placed into aluminum pans and tested in nitrogen atmosphere in a Q1000 calorimeter (TA Instruments). The first step in the thermal treatment was always annealing at 230 °C for 3 min to erase earlier thermomechanical histories. Next, samples were cooled to room temperature at a constant cooling rate of 10 °C /min.

Before identifying peak positions and determining crystallinity, a linear baseline was subtracted from the measured heat flow as a function of the temperature. Finally, crystallinity could be estimated as $X^{\mathrm{DSC}} = \Delta H_c/\Delta H_c^0$, where $\Delta H_c = \int_{T_s}^{T_e} (\mathrm{d}H/\mathrm{d}T)\mathrm{d}T$ and ΔH_c^0 are, respectively, the enthalpy of crystallization of the sample and the enthalpy of crystallization of an ideal 100% crystalline iPP sample (207.1 J g^{-1}).[24]

3. Results and Discussion

3.1. Effects of DMDBS on Structure and Morphology of iPP in the Solid State. It is well-known that a small amount of DMDBS can have a strong influence on structure and morphology of iPP.[10] Moreover, structure and morphology depend on crystallization conditions (thermal and mechanical histories). In order to isolate the effects due to the presence of DMDBS, we prepared our samples under the same crystallization conditions (quiescent crystallization with 10 °C/min). Figure 3 reports WAXD integrated intensities at room temperature for the neat iPP and the blends with DMDBS. The neat iPP shows the typical diffraction peaks of the α crystalline modification. When the additive is present, although the α form remains prevalent, the crystal structure of the polymer shows some specific changes. The 111 peak becomes better resolved and a broad 117 reflection appears. This indicates the simultaneous formation of less defected α and small γ crystals. However, we do not observe significant variation in the WAXD crystallinity index; in all cases, it lies around 60%. According to Foresta et al.,[34] the formation of γ-phase crystals in the presence of the nucleating agent can be explained from a thermodynamic point of view. In fact, the nucleating agent shifts the crystallization of the polymer at higher temperatures where nucleation of γ phase is favored and can compete with nucleation of the α phase. The ratio between γ and α phase crystals, X_γ, is estimated with

$$X_\gamma = \frac{A_{117}}{A_{130} + A_{117}} \quad (2)$$

where A_{130} and A_{117} are the areas of the nonoverlapping parts of the peaks 117 and 130. These two peaks were selected because they are the diagnostic reflections of the γ and the α phase, respectively. In the investigated range of concentration, the γ phase content, X_γ, is maximum for B03 ($X_\gamma = 0.15$) and drops for B07 ($X_\gamma = 0.09$) and B1 ($X_\gamma = 0.08$). This drop is probably related to a faster α nucleation rate at higher DMDBS concentrations.

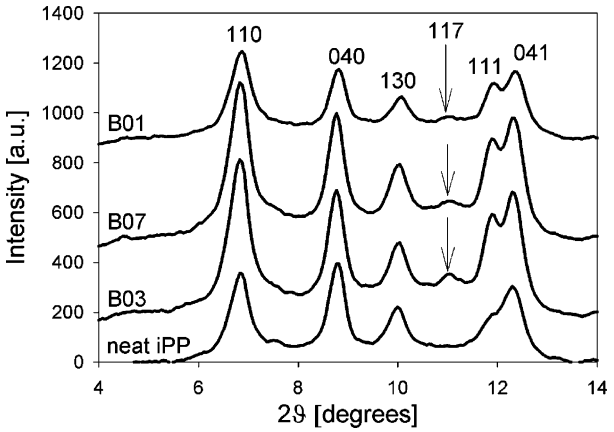

Figure 3. WAXD profiles of iPP at room temperature as a function of DMDBS concentration. All samples were prepared in the same conditions, i.e., crystallization from the melt at 10 °C/min. Presence of DMDBS induces the broad 117 peak, indicated by the arrow, that is associated with the formation of γ phase crystals. The crystallinity index is ∼60% in all cases while the amount of γ phase decreases with DMDBS concentration. Note that curves are shifted in the vertical direction for clarity.

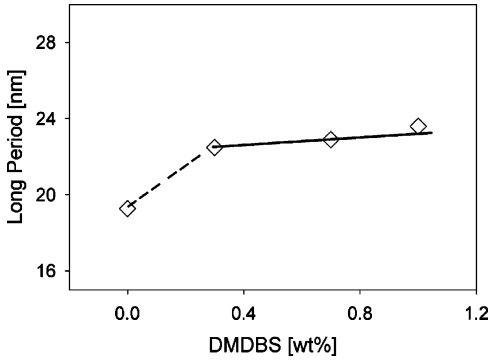

Figure 4. Long periods of iPP lamellae at room temperature as a function of DMDBS concentration. All samples were prepared under the same conditions, i.e., crystallization from the melt at 10 °C/min. The neat iPP shows a long period of 19 nm and this value rises to ∼23 nm for samples containing DMDBS. This increase in the long period is due to the formation of thicker crystals in the presence of DMDBS.

On the morphological side, the long period of iPP lamellae shows pronounced changes as a function of DMDBS concentration going from 19 nm of the neat sample to 23 nm (average value) of samples containing DMDBS, see Figure 4. Taking into account that the lamellar thickness, T_L, can be expressed as $T_L = L_p x$ and that the crystallinity index does not vary, our experimental observations are consistent with the formation of thicker crystals when DMDBS is present. The reason for this increase in crystal thickness is attributed to the higher crystallization temperature in the presence of the nucleating agent[8] that is discussed hereafter.

3.2. Crystallization under Quiescent Conditions. When cooling a homogeneous mixture of iPP and DMDBS to room temperature, two phase transitions are observed: crystallization of DMDBS and crystallization of the polymer. DSC experiments reveal the temperatures and enthalpies characterizing all these transitions. In fact, in the cooling thermograms of Figure 5, the crystallization peaks of the polymer are, in all cases, clearly visible and a closer look discloses another, much smaller, exotherm at higher temperatures. This smaller exotherm is associated with the crystallization of DMDBS and, due to the small amount of the additive, becomes visible only after

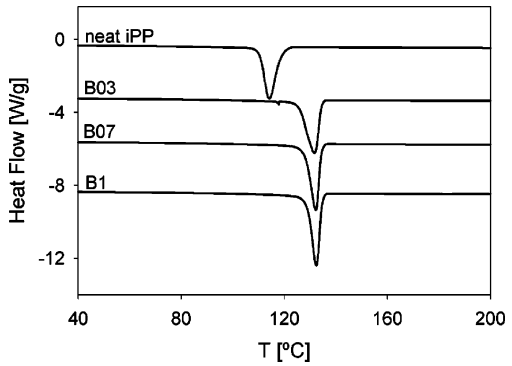

Figure 5. DSC cooling thermograms (after subtraction of a linear baseline) for the neat polymer and blends B03, B07, and B1. Experiments were performed at 10 °C/min, in an N_2 atmosphere, after annealing the samples at 250 °C for 3 min. Curves are shifted along the vertical axis for clarity. Clearly, with the addition of 0.3 wt % of DMDBS, the crystallization peak shifts to higher temperature, 132 °C. The peak does not change with further addition of the additive. Nevertheless, the crystallization peak becomes narrower when increasing the amount of DMDBS.

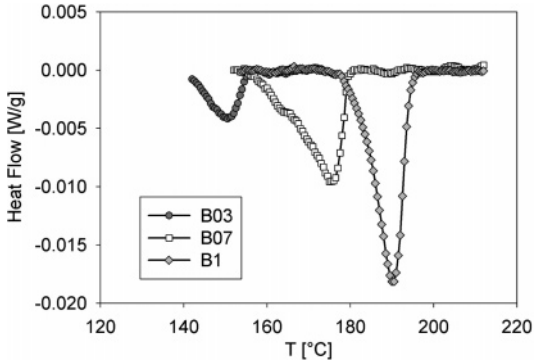

Figure 6. Magnification of the cooling experiments of Figure 5 in the temperature range preceding the crystallization of the polymer. The small exotherms are associated with the crystallization of DMDBS. As expected, latent heat of crystallization and peak temperature increase with DMDBS concentration. For clarity, the curves are shifted to the same baseline.

Table 1. Summary of Experimental Data Obtained from DSC Data Shown in Figure 5[a]

	T_{peak}^{DSC} [°C]	T_{onset}^{DSC} [°C]	ΔH [J g^{-1}]	t_c [s]	T_{ps}^{DSC} [°C]	X^{DSC} [%]
HD120MO	113	120	95.3	123.5		46
0.3% DMDBS−B03	131	135	107.7	68.5	149	52
0.7% DMDBS−B07	132	135	107.7	53.6	175	52
1% DMDBS−B1	132	135	103.5	47.3	189	50

[a] T_{peak}^{DSC} and T_{onset}^{DSC} represent peak and onset temperature of the exotherm associated to crystallization of the polymer, t_c is the crystallization time defined as $t_c = ((T_{onset}^{DSC} - T_{compl}^{DSC})/(dT/dt))$ where T_{compl}^{DSC} corresponds to the completion of the crystallization and dT/dt is the cooling rate (= 10 °C/min), T_{ps}^{DSC} represents the peak temperature of the exotherm associated to DMDBS crystallization, X^{DSC} is the degree of crystallinity of the polymer.

sufficient magnification, see Figure 6. Table 1 summarizes the relevant DSC data during cooling experiments. Note that these data provide enough information to sketch the phase diagram of the system in the investigated range of concentration. Upon addition of 0.3 wt % of DMDBS, the crystallization temperature (peak value) of iPP, T_c, increases to 131 °C. Further addition of DMDBS has nearly no effect on T_c that is 132 °C for both B07 and B1. Nevertheless, the crystallization peak of the polymer narrows at higher DMDBS contents indicating faster crystallization. Saturation of T_c of iPP with DMDBS concentration was observed also by Kristiansen et al.;[10] in their data, T_c reaches ~130 °C at 0.4 wt % DMDBS. Increasing the DMDBS concentration, the phase separation occurs at increasingly higher temperatures. In accordance with WAXD, the final crystallinity of iPP is hardly affected by DMDBS. However, the values measured by DSC, namely, 50%, are noticeably lower than those found with WAXD.

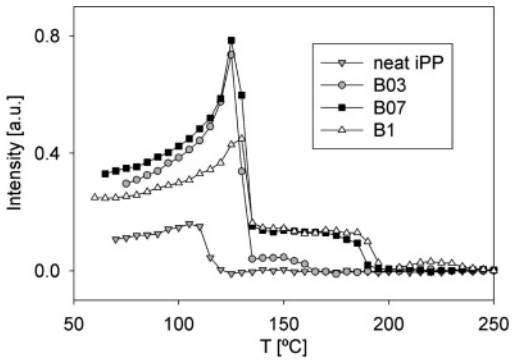

Figure 7. Temperature dependence of the SAXS intensity as a function of DMDBS concentration during cooling at 10 °C/min and after annealing at 250 °C for 3 min. In samples containing DMDBS, the scattered intensity increases with phase separation because of density fluctuations between DMDBS crystals and the polymer. At lower temperatures, when the polymer crystallizes once again, the scattered intensity increases.

Table 2. Summary of the SAXS Data Obtained from Figure 8[a]

	T_c^{SAXS} [°C]	T_{peak}^{SAXS} [°C]	$T_{onset\ ps}^{SAXS}$ [°C]	$T_{plateau}^{SAXS}$ [°C]
HD120MO	120	108		
0.3% DMDBS−B03	135	125	165	150
0.7% DMDBS−B03	135	125	190	175
1% DMDBS−B1	135	127	195	185

[a] T_c^{SAXS} and T_{peak}^{SAXS} are, respectively, the onset temperature for polymer crystallization and the temperature corresponding to the maximum scattered intensity, $T_{onsetps}^{SAXS}$ is the onset temperature for DMDBS phase separation, and $T_{plateau}^{SAXS}$ is the temperature at which the intensity reaches a constant value (above T_c).

Information on the morphology of the system as a function of the temperature is obtained by means of SAXS. Figure 7 shows the integrated scattered intensity as a function of the temperature for the neat iPP and the blends with DMDBS. These data can be interpreted remembering that SAXS intensity is the result of density fluctuations. As expected, in the neat iPP there is no density fluctuation until the polymer starts nucleating around 120 °C, while samples containing DMDBS show more complicated temperature dependence. In fact, when phase separation occurs, hydrogen-bonding drives DMDBS molecules to pile up and form crystals denser than the polymer. As a consequence, density fluctuations are established and the scattered intensity rises to a plateau. At lower temperature, around 135 °C, independently from DMDBS concentration, nucleation of the polymer triggers a large and abrupt upturn in the intensity. Similar to DSC, some characteristic temperatures for the crystallization of the polymer and of the additive are located and reported in Table 2. These data are used to build the phase diagram shown in Figure 8 that is used as reference in the rest of this work. In accordance with Kristiansen et al.,[10] three different regions, corresponding to three different physical states of the system, are identified: (1) Region I, at high temperatures DMDBS and iPP form a homogeneous solution; (2) Region II, at intermediate temperatures, the system is phase separated with DMDBS crystallized and iPP still molten; (3) Region III, at low temperatures both DMDBS and iPP are crystallized.

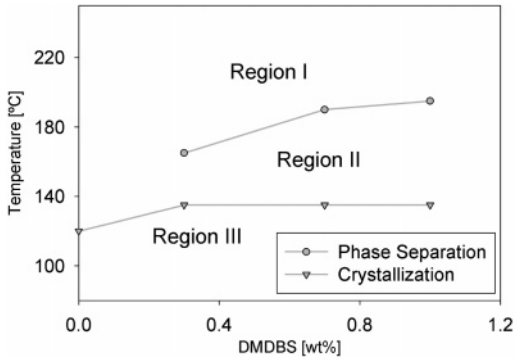

Figure 8. Phase diagram of the system iPP−DMDBS (from 0 to 1 wt % DMDBS) obtained, on cooling, using SAXS data. Three regions corresponding to three different states can be identified: Region I, homogeneous liquid; Region II, phase separated system with crystallized DMDBS and molten polymer, and Region III, both iPP and DMDBS are crystallized.

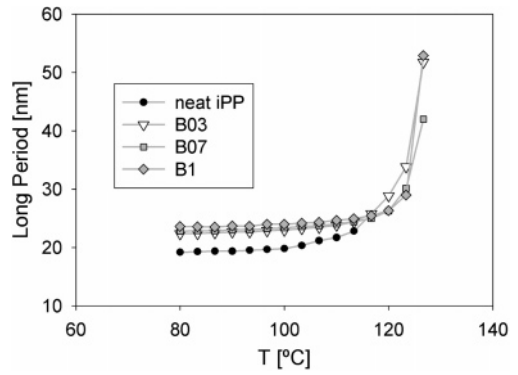

Figure 9. Long period as a function of temperature and DMDBS concentration during temperature ramps with a cooling rate of 10 °C/min. Presence of DMDBS leads to an increase of the long periods that below 80 °C is quantified in ∼4 nm.

When the polymer crystallizes, in Region III, SAXS allows for the measurement of the long period. Figure 9 shows the data concerning the neat polymer, B03, B07, and B1 as a function of temperature. As already discussed, the presence of DMDBS leads to an increase in L_p.

3.3. Morphology of the System in Region II. Two-dimensional SAXS images reveal that the increase of the integrated intensity in Region II is caused by an increase of the scattering in all azimuthal directions at low q. Sample images are shown in Figure 10. The increase in the scattering can be ascribed to the formation of a suspension of randomly oriented DMDBS fibrillar crystals with a length L and a radius R. In this case, the intensity scattered at low angles, $2\pi/L < q < 1/R_c$, can be described with[25−27]

$$I(q) = \frac{C}{q}\exp\left(-\frac{R_c^2 q^2}{2}\right) \qquad (3)$$

where C is a constant including details on the scatterers like concentration and electron density, while R_c is the radius of gyration of the cross section of the scatterers ($R_c = R/\sqrt{2}$). However, from the existing literature, it is known that DMDBS fibrils are basically endless ($L \rightarrow \infty$); therefore, eq 3 is valid for $q < 1/R_c$ in this case. Within this limit, $\log[I(q)q]$ versus q^2 is a straight line with a slope $-R_c^2/2$. Fitting eq 3 to the data points allows for the calculation of R_c and therefore of R. Figure 11 provides an example of such a fit demonstrating that a good agreement between experimental data and eq 3 exists for $0.15 < q < 0.3$ nm^{-1} (i.e., for $0.025 < q^2 < 0.1$ nm^{-2}). This observation is consistent with the presence of fibrillar scatterers with a radius of ∼4.5 nm and a length that exceeds the experimental accessible SAXS range ($L > 200$ nm). As shown in Figure 12, the radius of DMDBS fibrils is independent of DMDBS concentration. This result is in agreement with the findings of Thierry et al.[9] and Shepard et al.[12] of observed elementary (DBS) fibrils with a radius of ∼5 nm. It is also reported that elementary fibrils of DBS and DMDBS can form bundles with a radius of ∼50 nm at concentrations as low as 0.1 wt %[12,28] and that the population of bundles becomes larger increasing the additive content. From our SAXS experimental range, it is difficult to infer bundles formation; however, this could be the source of discrepancies observed between experimental data points and eq 3 in the low q range. For instance, in Figure 11, the agreement between data points and eq 3 ceases at $q^2 = 0.025$ nm^{-2} (i.e., at $q = 0.15$ nm^{-1}). The measured intensity is higher than what is predicted by eq 3, suggesting also the presence of thicker scatterers. For instance, if another linear region with a steeper slope could be identified at lower q values, this could indicate the presence of scatterers characterized by a radius $R = \sqrt{2}/0.15 = 9.5$ nm, i.e., bundles made of two elementary DMDBS fibrils. Unfortunately, with our experimental limits, this aspect is difficult to assess. With the detection of larger bundles of elementary DMDBS fibrils, it is even more difficult because the limit $q < 1/R_c$ proceeds rapidly toward too low values when the radius of the scatterers grows.

3.4. Rheology of the System in Region II. Phase separation of DMDBS has a strong influence on the rheology of the system. Relaxation times and moduli increase because of network formation. One way to determine the temperature where this change happens is to measure the storage modulus (G') at constant frequency during cooling from Region I. The data are shown in Figure 13. As expected, for the neat iPP, G' is only affected by the change in temperature. This implies linear (Arrhenius) behavior on a logarithmic scale.[22] At lower temperatures, when nucleation sets in, an abrupt upturn is observed. In contrast, G' of samples containing DMDBS exhibits a more complex temperature dependence. When DMDBS starts phase separating, G' rises quickly because of the growth of DMDBS fibrils and deviates from the linear behavior. After completion of the phase separation and before nucleation of the polymer, the linear dependence is restored. With increasing DMDBS concentration, the rise in G' becomes more pronounced because of the formation of a denser network that, in addition, includes more multiple fibril strands that are stiffer than the elementary fibrils. In line with DSC and SAXS, nucleation is observed at similar temperatures for samples containing DMDBS (∼138 °C), while, the neat iPP nucleates at a lower temperature (∼120 °C). The changes in the rheology with DMDBS phase separation are not fully described using only one frequency. Therefore, in Figure 14 the frequency dependent mechanical response of the neat iPP is compared with that of the blend B07, at 188 °C, after phase separation. Clearly, the transition from a melt to a suspension of DMDBS fibrils alters the values of both storage and loss modulus of iPP over at least five decades of frequencies. The phase separated system exhibits a G' higher than G'' in the entire experimental frequency window. Moreover, from ∼1 to ∼10 rad/s, G' and G'' display a power law dependence on the frequency (linear trend in a double logarithmic plot)[30,32] that, according to some authors, is the fingerprint of a fractal structure. Furthermore, in the phase separated system, G' shows a plateau in the low-frequency region that is associated with the formation of a percolated network[31] of DMDBS fibrils. The combination of the rheological features described above is

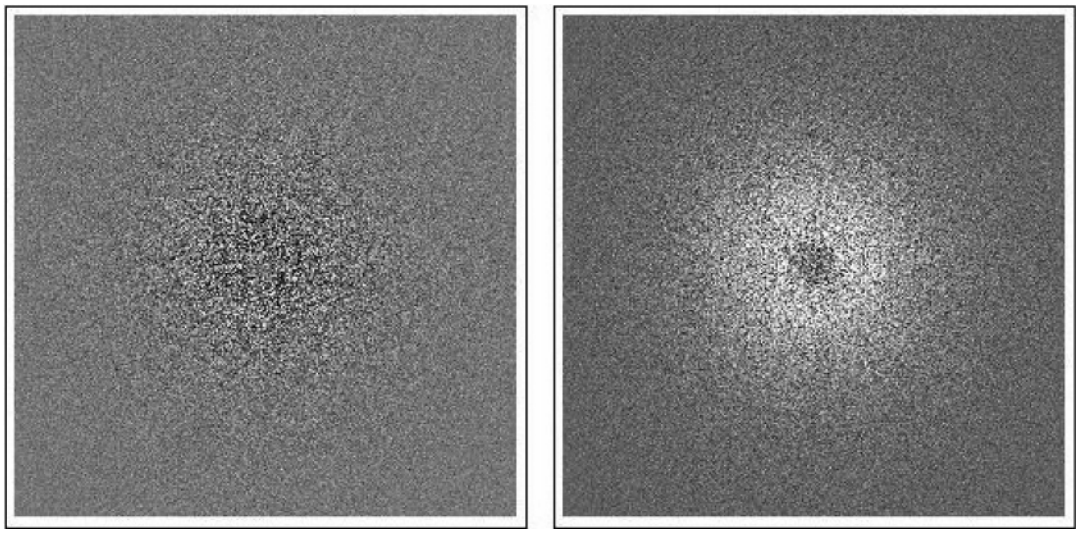

Figure 10. SAXS images of the blend B1. Left: material in Region I of the phase diagram. Right: material in Region II of the phase diagram. DMDBS phase separation causes an increase of the scattered intensity in all directions at low q values. For a clear visualization, the scattering of the system in Region I was subtracted.

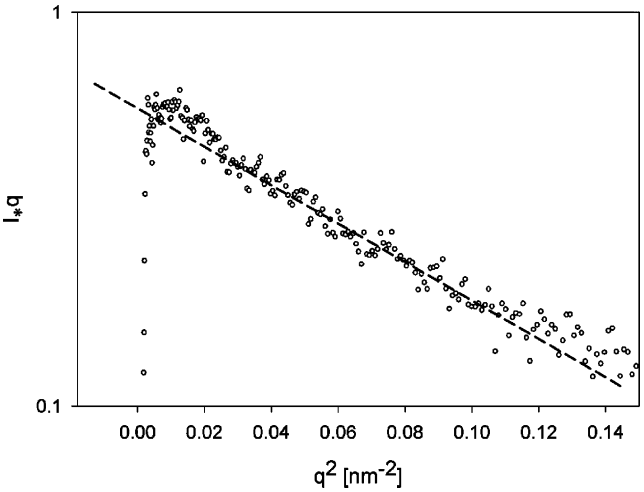

Figure 11. SAXS data points with a fit (− − − −) of eq 3 for the blend B1 in Region II. For endless fibrils, eq 3 holds in the limits: $q < 1/R_c$. The experimental data deviate from the dashed line at $q^2 \cong 0.1$ nm^{-2}, consistent with fibrils having a radius of 4.5 nm. At very low q, the agreement between eq 3 and the data ceases at $q^2 = 0.025$ nm^{-2}. This could be the fingerprint of bundles of elementary DMDBS fibrils.

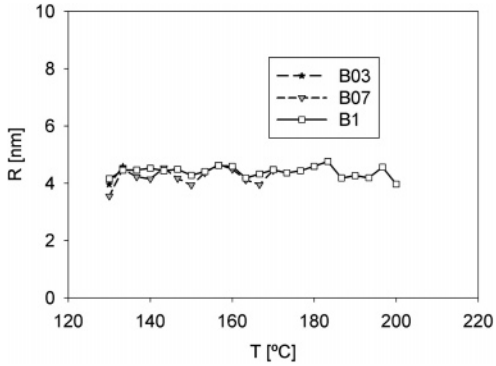

Figure 12. Radius of DMDBS fibrils as a function of temperature and DMDBS concentration. The data are obtained fitting eq 3 on the experimental data. For B07 and B1, phase separation starts at higher temperature than B03; therefore, more data points are available in these two cases. Independent of the DMDBS concentration, the average value is 4.5 nm.

typically associated to a gel beyond the critical gel stage.[29,30] The viscouslike response observed in the lowest-frequency region highlights the physical nature of the DMDBS fibrillar network. In other words, DMDBS fibrils are in contact but not permanently (chemically) bonded, and for this reason, they can still slide over each other but only at very long experimental times. As a result, the DMDBS network of fibrils slows down the relaxation of the melt with the introduction of new, long relaxation modes.

3.5. Effect of Flow on iPP−DMDBS Blends Near the Gel Transition. DMDBS phase separation changes the rheology of the system making relaxation slower. Therefore, we envisage that this transition influences the flow behavior of the system. In order to study the influence of shear flow on the DMDBS network of fibrils, the blend B1 was selected. According to rheology, the onset of phase separation for this blend, in quiescent conditions, is at 195 °C. Interestingly, we found that, even at 210 °C, application of a strong shear flow of 60 s^{-1} for 3 s causes immediate phase separation of the additive. In other words, shear enhances phase separation of DMDBS shifting the onset 15 °C above its "quiescent" value. Rheological data concerning this flow-induced phase separation are presented in Figure 15. Although the phase separation starts at higher temperatures with shear, the increase in the storage modulus is approximately the same as in the quiescent case. Furthermore, at the applied cooling rate (10 °C/min), the nucleation temperature of the polymer is not affected. When the same shear flow is applied after formation of a network of DMDBS fibrils, at 188 °C for instance, the scenario is different. Here, as shown in Figure 16, flow causes a drop in the storage modulus, larger than one decade, that does not heal during cooling. The physical nature of the DMDBS network is the cause of this drop. In fact, during shear, the fibrils are forced to slide over each other and tend to align parallel to the flow direction. As a consequence, the network breaks and the elastic modulus drops. Alignment of DMDBS fibrils causes a strong and anisotropic density fluctuation along the flow direction as depicted in Figure 17. This density fluctuation results in a streak of intensity in the equatorial region of SAXS images. In these circumstances, time-resolved SAXS is a valuable technique also for studying the relaxation times of the fibrils. As shown in Figure 18, the streak of intensity and therefore the alignment of the fibrils is retained without significant changes over the whole experimental time (> 2000 s). On the time scales characterizing the use of

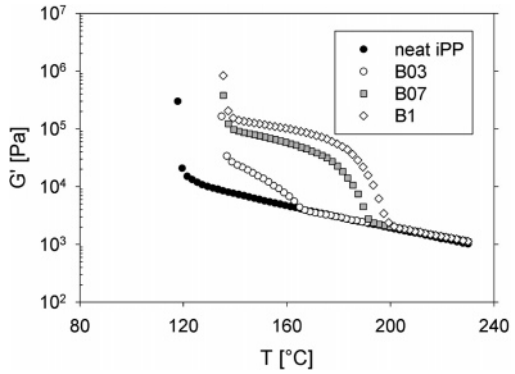

Figure 13. Storage modulus ($\omega = 5$ rad/s) as a function of temperature for the neat iPP and the blends B03, B07, and B1. Data points are recorded on cooling (rate 10 °C/min) after annealing in Region I. The neat iPP shows a thermorheological simple (Arrhenius) behavior in all the temperature range preceding the steep increase of G' because of nucleation. In the blends containing DMDBS, the thermorheological simple behavior is also observed at high temperatures (Region I). However, the transition to Region II leads to a more complex behavior with an extra increase of G' corresponding to the phase separation of DMDBS. This increase is ascribed to the growth of DMDBS fibrils with network formation. After completion of phase separation, the Arrhenius behavior is restored until the polymer nucleates in Region III. In Region II, higher DMDBS contents relate to larger increases in G' suggesting the formation of a denser network of fibrils.

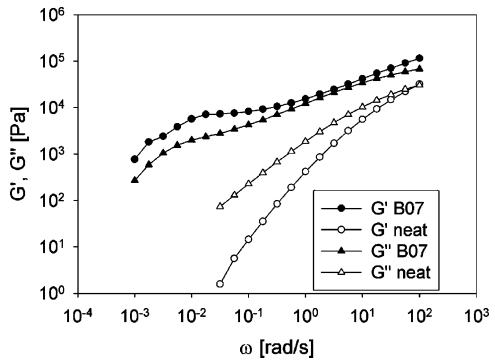

Figure 14. Storage and loss moduli (G' and G'') as a function of frequency at 188 °C for the neat iPP and B07 (annealed for 30 min). Both G' and G'' are higher in B07 than in the neat polymer. The formation of a percolated network of fibrils is responsible for the plateau in G' observed at low frequencies in B07. The physical nature of the network is unveiled by the viscouslike behavior visible in the lowest frequency range. This network contributes to slow down of the relaxation times of the system.

these materials in processing, the alignment of DMDBS fibrils can be considered as permanent.

3.6. Morphological Implications of Flow and DMDBS Phase Separation on the Crystallization of iPP. In section 3.2, we described the ability of DMDBS in nucleating iPP. Because of a favorable lattice matching, the energy barrier for heterogeneous nucleation on the surface of DMDBS fibrils is lower than the energy barrier for homogeneous nucleation. Therefore, most of the polymer "prefers" to nucleate on the DMDBS fibrils.

In section 3.5, we described the effect of shear on the network of DMDBS fibrils. For the blend B1, we found that a shear flow of 60 s^{-1} for 3 s, applied at a temperature a few degrees above the transition to Region II, can enhance the phase separation of the additive. In contrast, if the same shear is applied a few degrees below the transition to Region II, the fibrils align parallel to the flow and the network is broken. Similar results are also obtained for the blends B03 and B07. The flow induced morphology of iPP−DMDBS blends arises

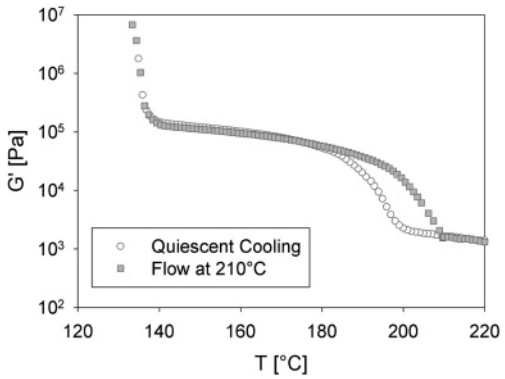

Figure 15. Temperature dependence for G' ($\omega = 5$ rad/s) of the blend B1 with and without the application of a shear flow (60 s^{-1} for 3 s) at 210 °C, in Region I of the phase diagram. Clearly, shear flow has the effect of enhancing the phase separation of the additive that, in this case, starts immediately after shearing. Nevertheless, after completion of the phase separation, the observed increase of G' is very close to the quiescent case. At lower temperatures, nucleation of the polymer occurs, unaffected by flow, at 138 °C.

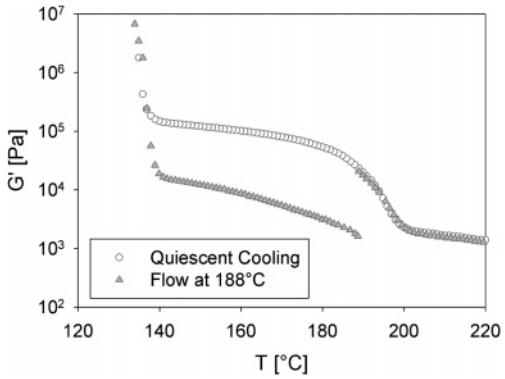

Figure 16. Temperature dependence for G' ($\omega = 5$ rad/s) of the blend B1 with and without the application of a shear flow (60 s^{-1} for 3 s) at 188 °C in Region II of the phase diagram, after DMDBS phase separation. Shear causes a large drop in G' that is not recovered even at lower temperatures. This drop can be explained with disconnection of the fibrillar network and alignment of the fibrils in the flow direction. Shear flow does not affect the nucleation of the polymer at lower temperatures.

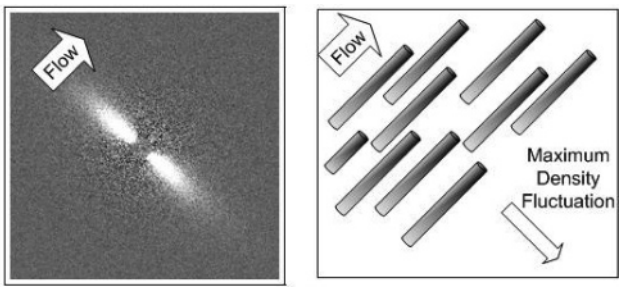

Figure 17. (Left) SAXS image showing a streak of intensity in the equatorial region. The image refers to the sample B1 after application of shear at 188 °C, in Region II. (Right) Schematic representation of DMDBS fibrils aligned parallel to the flow direction. An arrow indicates the direction corresponding to the maximum density fluctuation. This direction is orthogonal to the shear direction and parallel to the equatorial streak in the SAXS pattern.

from a combination of the physics described in sections 3.2 and 3.5.

The study of flow induced crystallization in iPP−DMDBS blends was carried out combining SAXS and a short-term shear protocol. The short-term shear protocol (with a shear of 60 s^{-1} for 3 s) was applied to the neat iPP and to the blends B03, B07, and B1 before and after phase separation of the additive.

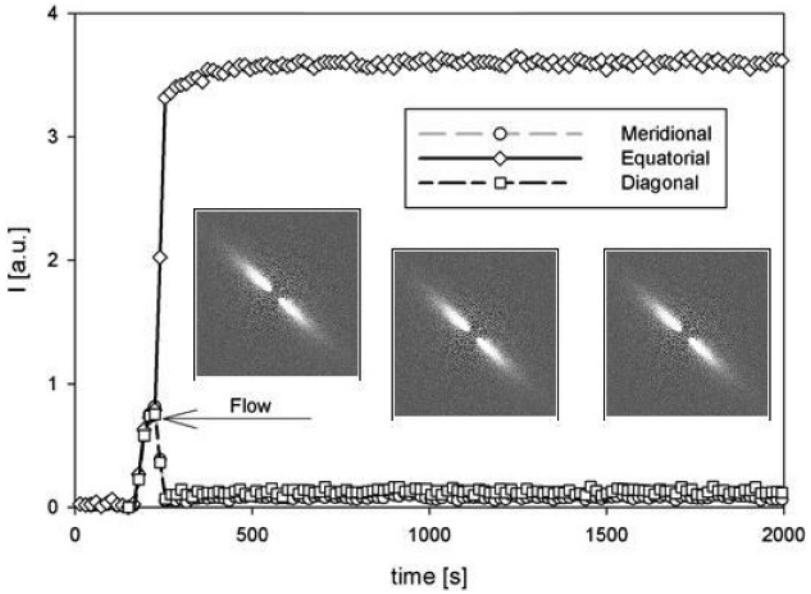

Figure 18. Time dependence of meridional, equatorial, and diagonal intensity of the blend B1 at 188 °C after application of shear flow (60 s^{-1} for 3 s). When phase separation takes place, around 100 s, the scattered intensity, as expected, rises evenly in all directions. Therefore meridional, equatorial, and diagonal intensities rise evenly. However, after application of shear flow, a streak of intensity appears in the equatorial region and, therefore, the intensity scattered in this region increases while it decreases in the meridional and diagonal regions. This situation arises due to alignment of DMDBS fibrils. The different intensity levels are retained for times longer than the experimental time without any significant changes. Inserted figures show SAXS images corresponding to increasing times.

Afterward, the polymer was allowed to crystallize by cooling to room-temperature.

The effects of flow in Region I (prior to the crystallization of DMDBS) were tested by applying shear to B03 at 185 °C, to B07 at 195 °C, and to B1 at 210 °C. Independent of the DMDBS concentration, shear in Region I can only enhance phase separation. Upon cooling to Region II, DMDBS fibrils form randomly oriented in space and the polymer, crystallizing on top of a randomly oriented substrate, displays an isotropic morphology. The morphologies obtained in these cases are similar to the crystallization in quiescent conditions.

In contrast, shear in Region II (after crystallization of DMDBS) aligns DMDBS fibrils parallel to the flow direction. By design, the lateral growth of polymer lamellae occurs orthogonally to the fibril axis. Therefore, once the fibrils are aligned, lamellae grow in the direction orthogonal to the applied flow. With this templating mechanism, in the early stages of crystallization the orientation of the substrate is transformed into orientation of polymer lamellae. Shearing B03 at 150 °C, B07 at 178 °C, and B1 at 180 °C yields oriented polymer morphologies after cooling below T_c.

In principle, the anisotropic polymer morphology, observed after applying shear in Region II, could also be ascribed to orientation of the polymer at these lower temperatures. To exclude this possibility, we benchmark the morphology by crystallizing the neat iPP after application of shear at 150 °C. This temperature is the lowest used for iPP−DMDBS blends and therefore the most favorable for obtaining an anisotropic morphology. In spite of that, after cooling below T_c, the polymer crystallizes with an isotropic pattern.

A visual summary of the performed experiments, including SAXS images at room temperature is given in Figure 19. SAXS images of the polymer crystallized after application of shear in region II show a clear separation of the intensities scattered in different azimuthal regions that corresponds to a high degree of lamellar orientation. The intensity scattered by oriented crystallites is $I_{or} = I_{Eq} + I_{Mer}$ where I_{Eq} and I_{Mer} are, respectively, the intensity scattered in the equatorial and meridional regions.

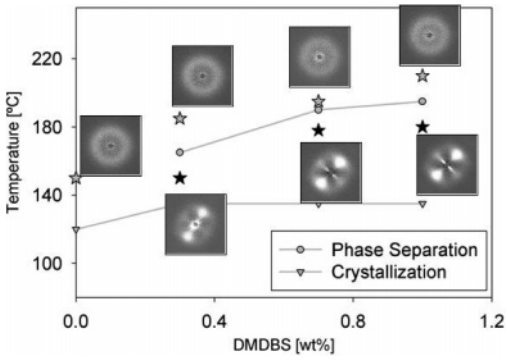

Figure 19. Phase diagram of iPP−DMDBS (from 0 to 1 wt % DMDBS) including SAXS images describing the morphology, at room temperature, after application of "short-term shear" protocol with shear temperatures indicated by the symbols (★). When shear flow is applied above the DMDBS phase separation (in Region I), isotropic polymer morphologies are obtained. In contrast, shear flow applied below the DMDBS phase separation (in Region II) yields polymer morphologies with a high degree of anisotropy.

Therefore, an assessment of the degree of orientation of polymer lamellae, Φ, can be obtained by combining the intensities scattered in the different azimuthal regions: $\Phi = (I_{Eq} + I_{Mer})/I_{Tot}$ where I_{Tot} is the total scattered intensity.[33] However, the scattering in the equatorial region also contains a contribution from the oriented DMDBS fibrils, I_{DMDBS}. Therefore, a better definition for the degree of orientation of the polymer lamellae is[17]

$$\Phi = \frac{(I_{Eq} + I_{Mer}) - I_{DMDBS}}{I_{Tot} - I_{DMDBS}} \quad (4)$$

I_{DMDBS} is taken as the value assumed by the equatorial intensity immediately before the crystallization of the polymer. The values of Φ, calculated at room temperature after application of shear in Region II, increase with DMDBS concentration and range from 0.4 of B03 to 0.6 of B1, see Figure 20. Similar values were reported by Nogales et al.[17] in experiments with a similar

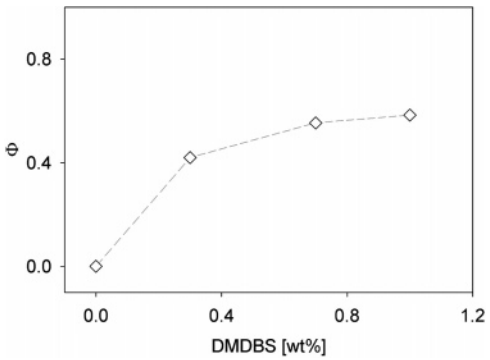

Figure 20. Orientation factor calculated with eq 4 as a function of DMDBS content measured at room temperature after the application of shear in Region II. The neat iPP showed no orientation; therefore, the corresponding value is set to 0. Samples containing DMDBS show increasingly high values of orientation.

protocol carried out on a propylene−ethylene copolymer and containing less than 1 wt % of DBS.

4. Conclusions

We studied the phase behavior of the binary system iPP−DMDBS for concentration of the additive ranging from 0 to 1 wt %. The results are in agreement with the monotectic behavior already reported. When the DMDBS phase separates, we addressed the formation of a percolated network of fibrils and the effects that this network has on the crystallization of the polymer. SAXS patterns are consistent with formation of DMDBS fibrils with a radius of ∼4.5 nm and a length exceeding the experimental range (L > 200 nm). It is known that the surface of these fibrils hosts a large number of nucleation sites for iPP, and because of a favorable epitaxy matching, iPP molecules tend to nucleate on this substrate. The epitaxial relation between iPP and DMDBS is such that polymer lamellae always grow in the radial direction starting from the surface of the fibrils. DMDBS assists nucleation of iPP reducing the energy barrier, and as a consequence, the crystallization temperature of the polymer raises as much as 19 °C. The growth of DMDBS fibrils within the molten iPP matrix gives rise to a physical network that changes the rheology of the system introducing long relaxation times. This change becomes more pronounced at higher DMDBS concentration and, as expected, affects the flow induced crystallization.

When no flow is applied, DMDBS fibrils form with a random orientation in space and, therefore, iPP lamellae grow following the same isotropic pattern. When flow is applied two situations are discussed: (1) If flow is applied before the DMDBS phase separates, then the fibrils form in absence of strain and adopt the ordinary random orientation in space. For this reason, crystallization of iPP occurs with an isotropic morphology. (2) If flow is applied after DMDBS phase separation, the imposed deformation drives DMDBS fibrils parallel to the flow direction. When iPP nucleates, lamellae grow as usual with the *c*-axis parallel to the fibrils axis, and therefore parallel to the flow direction. Oriented shish kebab morphologies are generated where the core is made of DMDBS and the kebabs by iPP. Polymer morphologies characterized by a high degree of anisotropy are obtained even though, in some cases, flow is applied well above the melting point of the polymer, i.e., in absence of undercooling.

Summarizing, we show that, when iPP nucleates, lamellar orientation is determined by the orientation of the DMDBS fibrils. This peculiarity can be used to template (assisted by epitaxy matching) the orientation of polymer lamellae. The phase separation of DMDBS can be seen as a switching mechanism for obtaining highly oriented iPP morphologies after application of flow at high temperatures. In summary, we conclude that when DMDBS is present, thermomechanical history has a marked effect on iPP morphology. A critical condition exists for the transition from isotropic to oriented morphology: phase separation of DMDBS. The location of this critical condition in the phase diagram is set by the amount of DMDBS in the blend.

Acknowledgment. The authors are indebted to the personnel of BM26/DUBBLE and ID11 and especially to Dr. G. Heunen for assistance during the X-ray experiments. Furthermore, NWO (Nederlandse Organisatie voor Wetenschappelijk Onderzoek) and ESRF are acknowledged for granting the beamtime. This work is part of the Research Programme of the Dutch Polymer Institute (DPI), P.O. Box 902, 5600 AX Eindhoven, The Netherlands, Project No. 132.

References and Notes

(1) Schrauwen, B. A. G.; Breemen, L. C. A. v.; Spoelstra, A. B.; Govaert, L. E.; Peters, G. W. M.; Meijer, H. E. H. *Macromolecules* **2004**, *37*, 8618−8633.
(2) Kristiansen, M.; Tervoort, T.; Smith, P.; Goossens, H. *Macromolecules* **2005**, *38*, 10461−10465.
(3) Binsbergen, F. L. *Nature* **1966**, *211*, 516−517.
(4) Devaux, N.; Monasse, B.; Haudin, J. M.; Moldenaers, P.; Vermant, J. *Rheol. Acta* **2004**, *43*, 210−222.
(5) Kobayashi, T.; Hashimoto, T. *Bull. Chem. Soc. Jpn.* **2005**, *78*, 218−235.
(6) Blomehofer, M.; Ganzleben, S.; Hanft, D.; Schmidt, H. W.; Kristiansen, M.; Smith, P.; Stoll, K.; Mader, D.; Hoffmann, K. *Macromolecules* **2005**, *38*, 3688−3695.
(7) Zhu, P. W.; Edward, G. *Macromol. Mater. Eng.* **2003**, *288*, 301−311.
(8) Zhu, P. W.; Tung, J.; Edward, G. *Polymer* **2005**, *46*, 10960−10969.
(9) Thierry, A.; Fillon, B.; Straupe, C.; Lotz, B.; Wittmann, J. C. *Progr. Colloid Polym. Sci.* **1992**, *87* (31), 28−31.
(10) Kristiansen, M.; Werner, M.; Tervoort, T.; Smith, P.; Blomehofer, M.; Schmidt, H. W. *Macromolecules* **2003**, *(36)*, 5150−5156.
(11) Fillon, B.; Lotz, B.; Thierry, A.; Wittmann, J. C. *J. Polym. Sci., Part B: Polym. Phys.* **1993**, *31*, 1395−1405.
(12) Shepard, T. A.; Louth, R. M.; Walborn, J. L.; Norman, D. A.; Harvey, N. G.; Spontak, R. J. *J. Polym. Sci., Part B: Polym. Phys.* **1997**, *35*, 2617−2628.
(13) Marco, C.; Ellis, G.; Gomez, M. A.; Arribas, J. M. *J. Appl. Polym. Sci.* **2002**, *84*, 2440−2450.
(14) Nagarajan, K.; Levon, K.; Merson, A. S. *J. Therm. Anal. Calorim.* **2000**, *59*, 497−508.
(15) Dumitras, M.; Friedrich, C. *J. Rheol.* **2004**, *48* (5), 1135−1146.
(16) Fahrlander, M.; Fuchs, K.; Friedrich, C. *J. Rheol.* **2000**, *44* (5), 1103−1119.
(17) Nogales, A.; Mitchell, G. R. *Polymer* **2005**, *46*, 5615−5620.
(18) Nogales, A.; Mitchell, G. R.; Vaughan, A. S. *Macromolecules* **2003**, *36*, 4898−4906.
(19) Somani, R. H.; Yang, L.; Hsiao, B. S.; Agarwal, P. K.; Fruitwala, H. A.; Tsou, A. H. *Macromolecules* **2002**, *35*, 9096−9104.
(20) Hindeleh, A. M.; Johnson, D. J. *J. Phys. D: Appl. Phys.* **1971**, *4*, 259−263.
(21) Wang, Z. G.; Hsiao, B. S.; Sirota, E. B.; Srinivas, S. *Polymer* **2000**, *41*, 8825−8832.
(22) Macosko, C. *Rheology: Principles, Measurements, and Applications*; VCH: Weinheim, Germany, 1994.
(23) Pogodina, N. V.; Winter, H. H.; Srinivas, S. *J. Polym. Sci., Part B: Polym. Phys.* **1999**, *37*, 3512−3519.
(24) Wunderlich, B. *Macromolecular Physics*; Academic Press: New York, 1980.
(25) Guinier, A.; Fournet, G. *Small-Angle Scattering of X-rays*; Chapman & Hall: London, U.K., 1955.
(26) Chen, E.; Weng, X.; Zhang, A.; Mann, I.; Harris, F. W.; Cheng, S. Z. D.; Stein, R.; Hsiao, B. S.; Yeh, F. *Macromol. Rapid. Commun.* **2001**, *22*, 611−615.
(27) Glatter, O.; Kratky, O. *Small Angle X-ray Scattering*; Academic Press: London, U.K., 1982.
(28) Lipp, J.; Shuster, M.; Terry, A. E.; Cohen, Y. *Langmuir* **2006**, *22* (14), 6398−640.
(29) Mours, M.; Winter, H. H. *Macromolecules* **1996**, *29*, 7221−7229.

(30) Winter, H. H.; Mours, M. *Adv. Polym. Sci.* **1997**, *134*, 165−234.

(31) Coppola, S.; Acierno, S.; Grizzuti, N.; Vlassopoulos, D. *Macromolecules* **2006**, *39*, 1507−1514.

(32) Takenaka, M.; Kobayashi, T.; Saijo, K.; Tanaka, H.; Iwase, N.; Hashimoto, T.; Takahashi, M. *J. Chem. Phys.* **2004**, *121* (7), 3323−3328.

(33) Somani, R. H.; Hsiao, B. S.; Nogales, A.; Srinivas, S.; Tsou, A. H.; Sics, I.; Balta-Calleja, F. J.; Ezquerra, T. A. *Macromolecules* **2000**, *33*, 9385−9394.

(34) Foresta, T.; Piccarolo, S.; Goldbeck-Wood, G. *Polymer* **2001**, *42*, 1167−1176.

MA071460G